AGU PUBLICATIONS

Paleoceanography

RESEARCH ARTICLE
10.1002/2015PA002860

Key Points:
- Export production fluctuated over the past 4.3 Ma in EEP
- Orbital time and long-term export production control mechanisms are different
- Correlation between export production and climate changed around 1.1 Ma

Supporting Information:
- Texts S1–S3 and Figures S1–S5
- Table S1

Correspondence to:
A. Paytan,
apaytan@ucsc.edu

Citation:
Ma, Z., A. C. Ravelo, Z. Liu, L. Zhou, and A. Paytan (2015), Export production fluctuations in the eastern equatorial Pacific during the Pliocene-Pleistocene: Reconstruction using barite accumulation rates, *Paleoceanography*, *30*, 1455–1469, doi:10.1002/2015PA002860.

Received 15 JUL 2015
Accepted 2 OCT 2015
Accepted article online 14 OCT 2015
Published online 11 NOV 2015

©2015. American Geophysical Union. All Rights Reserved.

Export production fluctuations in the eastern equatorial Pacific during the Pliocene-Pleistocene: Reconstruction using barite accumulation rates

Zhongwu Ma[1,2], Ana Christina Ravelo[2], Zhonghui Liu[3], Liping Zhou[1,4], and Adina Paytan[2]

[1]Laboratory for Earth Surface Processes, Department of Geography, Peking University, Beijing, China, [2]University of California Santa Cruz, Santa Cruz, California, USA, [3]Department of Earth Sciences, University of Hong Kong, Hong Kong, [4]Institute of Ocean Research, Peking University, Beijing, China

Abstract Export production is an important component of the carbon cycle, modulating the climate system by transferring CO_2 from the atmosphere to the deep ocean via the biological pump. Here we use barite accumulation rates to reconstruct export production in the eastern equatorial Pacific over the past 4.3 Ma. We find that export production fluctuated considerably on multiple time scales. Export production was on average higher (51 g C m^{-2} yr^{-1}) during the Pliocene than the Pleistocene (40 g C m^{-2} yr^{-1}), decreasing between 3 and 1 Ma (from more than 60 to 20 g C m^{-2} yr^{-1}) followed by an increase over the last million years. These trends likely reflect basin-scale changes in nutrient inventory and ocean circulation. Our record reveals decoupling between export production and temperatures on these long (million years) time scale. On orbital time scales, export production was generally higher during cold periods (glacial maxima) between 4.3 and 1.1 Ma. This could be due to stronger wind stress and higher upwelling rates during glacial periods. A shift in the timing of maximum export production to deglaciations is seen in the last ~1.1 million years. Results from this study suggest that, in the eastern equatorial Pacific, mechanisms that affect nutrient supply and/or ecosystem structure and in turn carbon export on orbital time scales differ from those operating on longer time scales and that processes linking export production and climate-modulated oceanic conditions changed about 1.1 million years ago. These observations should be accounted for in climate models to ensure better predictions of future climate change.

1. Introduction

Phytoplankton can influence climate by sequestering atmospheric CO_2 via the biological pump; in turn, climate-driven changes in ocean circulation and mixing and/or in nutrient inputs from land (dust deposition and weathering) can affect ocean productivity and phytoplankton species distribution [*Jickells et al.*, 2005; *Wolff et al.*, 2006]. Specifically, changes in the efficiency of the biological pump, a process that removes CO_2 from the atmosphere-surface ocean pool, and changes in upwelling, a process that provides nutrients to fuel productivity but also releases CO_2 from the deep ocean into the atmosphere, may respond to and/or provide feedbacks in the climate system [*Cane*, 1998, 2005; *Chavez and Barber*, 1987; *Falkowski et al.*, 1998; *Turk et al.*, 2001]. The increasing concern of future climate warming has emphasized the need to understand the interactions between productivity, ocean chemistry, pCO_2, and climate, to allow for better representation of climate ecosystem interactions in predictive models [*Cox et al.*, 2000; *Schneider et al.*, 2008]. Two components of oceanic productivity are of particular interest: net primary production (NPP) and export production (the fraction of NPP that leaves the surface ocean and sinks to the deep ocean). The former is of interest for learning about oceanic ecosystems and carbon and nutrient cycling within the euphotic zone, while the latter is important for deciphering carbon sequestration in the deep ocean and the contribution of the biological pump to climate change [*Falkowski et al.*, 2003].

The Eastern Equatorial Pacific (EEP) is particularly important for understanding the links between climate and ocean productivity because a large fraction of global export production is associated with this upwelling region [*Kemp*, 1995]. This area of upwelling is also responsible for much of the CO_2 efflux from the ocean to the atmosphere [*Loubere*, 2000; *Pennington et al.*, 2006]. At present, the water upwelling in the EEP from about 60 to 100 m depth is cold and nutrient and CO_2 rich; the thermocline and nutricline depths in this area are tightly coupled; hence, increases in upwelling rate result in increases in productivity and decreases in sea surface temperatures (SST) [*Bjerknes*, 1969; *Cane*, 1998; *Turk et al.*, 2001]. Oceanographic processes which impact

the carbon cycle and climate within this region operate on subdecadal (e.g., El Nino), millennial (e.g., little ice age), orbital (e.g., glacial/interglacial), and geological (e.g., Pleistocene) time scales [*Pennington et al.*, 2006], and the processes that control ocean productivity and hence productivity-climate interaction on these various time scales may be distinct.

Reorganizations in ocean circulation, export production, and climate history are reflected in the sedimentary record in the EEP [*Kemp*, 1995; *Mayer et al.*, 1985, 1992; *Van Andel*, 1975]. Specifically, because of the relatively high proportional contribution of the EEP region to total ocean productivity and associated implications for climate, considerable effort has been devoted to the study of paleoproductivity, and fluctuation of productivity and export production in this region at multiple time scales have been reported [*Calvo et al.*, 2011; *Dekens et al.*, 2007; *Diester-Haass et al.*, 2006; *Etourneau et al.*, 2013; *Gartner et al.*, 1987; *King et al.*, 1998; *Lawrence et al.*, 2006; *Liu and Herbert*, 2004; *Mix et al.*, 2003; *Robinson et al.*, 2009; *Schneider and Schmittner*, 2006; *Steph et al.*, 2010]. To facilitate such reconstructions, a wide array of paleo-ocean productivity proxies have been utilized over the years. Notably, each of these proxies responds to different components of ocean productivity and may be affected by additional environmental variables [*Paytan*, 2009]. To shed light on the interaction between climate change and ocean export production and to better understand the processes that control these interactions, we have reconstructed export production in the EEP over the last 4.3 million years of Earth history using marine barite accumulation rates (BARs; see *Paytan and Griffith* [2007] and supporting information for information about BAR as a productivity proxy).

Over the last 4.3 million years, Earth has experienced a transition from warmer climates to cooler climates [*Haywood and Valdes*, 2004; *Ravelo et al.*, 2004] with the initiation of Northern Hemisphere glaciation (NHG) at ~3.6 Ma [*Mudelsee and Raymo*, 2005], further intensification of the NHG at ~2.75 Ma [*Haug et al.*, 1999], and a change in the dominant frequency of ice volume growth (shift from 41 k to 100 k) at ~1 Ma [*McClymont et al.*, 2013]. The mean global temperatures in the mid-Pliocene were ~3°C warmer than today [*Haywood and Valdes*, 2004], and pCO_2 was slightly higher than preindustrial levels (350–400 ppm) [*Pagani et al.*, 2010; *Seki et al.*, 2010]. The continental configuration and topography and large-scale ocean circulation patterns however were not much different than at present [*Haywood et al.*, 2011; *Zhang et al.*, 2012]. Most importantly, records of SST, ice volume (benthic $\delta^{18}O$), and other oceanographic and climatic parameters for this period and region are readily available and relatively well constrained [*Brierley et al.*, 2009; *Cannariato and Ravelo*, 1997; *Dekens et al.*, 2007; *Fedorov et al.*, 2010; *Ford et al.*, 2012; *Lawrence et al.*, 2006; *Mix et al.*, 1995; *Ravelo et al.*, 2004; *Steph et al.*, 2010; *Wara et al.*, 2005], allowing comparison of changes in export production to ocean/climate variability. Specifically, it has been suggested that intensification of the NHG and strengthening of the trade winds, over this time interval, resulted in lowering SST and shoaling of the thermocline in the EEP [*Dekens et al.*, 2007; *Ford et al.*, 2012; *Lawrence et al.*, 2006; *Steph et al.*, 2006, 2010]. The fact that changes in productivity seem to be decoupled from these changes in SST and thermocline [*Dekens et al.*, 2007; *Etourneau et al.*, 2013; *Lawrence et al.*, 2006] warrants further investigation and quantification of changes in export production.

Here we reconstruct export production using BAR at Ocean Drilling Program (ODP) site 849, which is situated today within the center of the EEP cold tongue. The coupling or decoupling between export production, SSTs, and climate-related changes on multiple time scales is evaluated by comparing our BAR record to available regional temperature records, the $\delta^{18}O$ record of global ice volume changes, and other published records of productivity changes. Using these records, we investigate the interplay between oceanographic processes modulating the C cycle and Earth's climate. Specifically, changes in upwelling strength, regional circulation, and nutrient redistribution in the ocean [*Matsumoto et al.*, 2002; *Sarmiento et al.*, 2004] and the efficiency of the biological pump and respective CO_2 efflux and C sequestration are considered.

2. Methods

2.1. Site Description

Samples were obtained from Ocean Drilling Program Leg 138 Site 849 situated at 0°11′N, 110°31′W, in the EEP cold tongue. The water depth at this site is 3851 m, and the sea floor has been above the carbonate compensation depth for the past 12 Ma [*Mix et al.*, 1995]. Site 849 sits beneath the westward flowing South Equatorial Current (SEC), and surface water circulation is influenced by the westward blowing trade winds [*Farrell et al.*, 1995] (Figure 1). Subsurface nutrient-rich water supplied from the equatorial undercurrent in this area upwells from no more than ~100 m depth [*Bryden and Brady*, 1985]. This nutrient-rich water

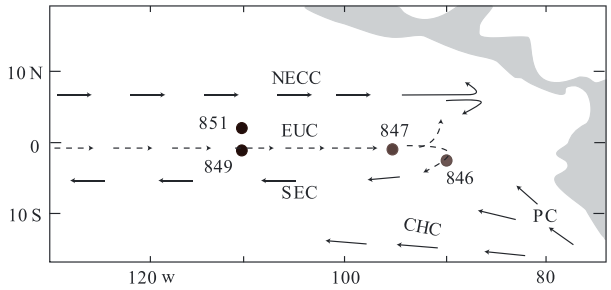

Figure 1. Map of the EEP region displaying ODP site 849 used in this study. ODP Sites 846, 847, and 851 in the eastern equatorial Pacific mentioned in our paper are also shown in this figure. Arrowheads show the major equatorial current systems. CHC = Chile Currents; PC = Peru Current; SEC = South Equatorial Current; EUC = Equatorial Undercurrent; NECC = North Equatorial Countercurrent; NEC = North Equatorial Current. Map modified from *Mix et al.* [1995].

is characterized by an annual mean SST that is about 4°C colder than the surrounding regions and supports high biological productivity [*Chavez and Barber*, 1987; *Fiedler et al.*, 1991].

Site 849 is composed of one lithologic unit of diatom nannofossil ooze with interbeds of nannofossil diatom ooze. Nannofossil and diatoms dominate the sediments, and foraminifers are common in the upper 100 m. Carbonate percentages are high but variable through most of the sequence. Sedimentation rates at this site are relatively high (~2–5 cm kyr^{-1}), and glacial/interglacial variability is not obscured by bioturbation [*Farrell et al.*, 1995].

2.2. Age Model

The age model for this site [*Shackleton et al.*, 1995], developed by using high-resolution gamma ray attenuation porosity evaluator density variations adjusted with magnetostratigraphy and biostratigraphy, was refined using benthic oxygen isotopes by *Mix et al.* [1995]. The age model was based on the revised meters composite depth (rmcd) [*Hagelberg et al.*, 1995]; however, we used the meters composite depth (mcd) scale because the differences in absolute depth for any given sample between the scales are small, generally on the order of centimeters. We have taken samples from the upper 120 mcd at ~50 cm intervals representing the past 4.3 Ma, which results in a temporal resolution of at least 20 kyr. In addition, sediments ranging in age between 120 and 340 kyr (3.75 mcd to 11.05 mcd) were sampled with a higher resolution of ~2 kyr covering two glacial cycles. We also sampled three segments (0.5 to 0.9 Ma, 1.2 to 2.1 Ma, and 3.2 to 3.9 Ma) at a slightly higher temporal resolution averaging around 13 kyr.

2.3. Weight Percent Barite

About 20 g of dry sediment was used for barite separation, depending on sample availability. A sequential leaching procedure was used to remove all sedimentary components except barite and a small amount of other refractory materials [*Eagle et al.*, 2003; *Paytan et al.*, 1996]. Barite recovery (yield) in this process is better than 90% [*Eagle et al.*, 2003; *Gonneea and Paytan*, 2006]. Samples with weight percent barite close to the method detection limits were listed as the value of the detection limit 2 mg. Sample residues were scanned using a scanning electron microscope with energy-dispersive spectrometry, and barite typically consisted of more than 95% of the sample. Based on crystal morphology and sulfur isotope ratios, no diagenetic barite was present in this core [*Markovic et al.*, 2015]. Values of weight percent barite were determined based on the fraction of barite recovered from the initial dry sediment used (Table S1 in the supporting information).

2.4. Weight Percent Carbonate

We determined calcium carbonate content (reported as weight percent $CaCO_3$) on 10 to 20 mg samples of bulk sediment using a UIC, Inc., Coulometrics Model 5012 CO_2 coulometer. Weight percent carbonate was calculated from the fraction of total inorganic carbon. Relative standard deviations on the means were always less than 1% for multiple determinations of a pure calcium carbonate standard, for samples run in duplicate within a given analytical run and for replicate analyses of the two consistency standards over all analytical runs reported here. The detection limit for weight percentage $CaCO_3$ for our samples was 0.5 wt %.

2.5. Mass Accumulation Rates

Mass accumulation rates (MAR) of barite (BAR, mg cm^{-2} kyr^{-1}) and $CaCO_3$ (carbon accumulation rate, g cm^{-2} kyr^{-1}) were calculated from their abundance in each sample, the linear sedimentation rate (LSR, m Ma^{-1}), and the dry bulk density (DBD, g cm^{-3}) (Figure 2). For example, BAR was calculated as BAR = [ppm barite × LSR × DBD]/10,000. The LSR was based on the age model for this site. Sample age was

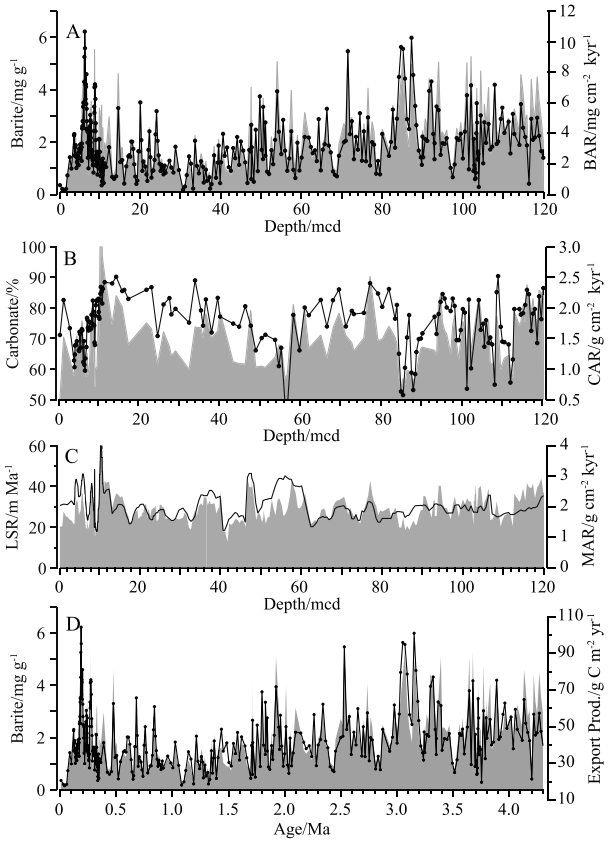

Figure 2. (a) Barite abundance (solid line with dots) and barite accumulation rates (represented as gray shaded area); (b) carbonate abundance (solid line with dots) and carbonate accumulation rates (represented as gray shaded area); and (c) the linear sedimentation rates (LSR, solid line) and mass accumulation rates (MAR represented as gray shaded area) plotted against depth at Site 849, as well as (d) barite abundance (solid line with dots) along with BAR-derived export production plotted against age at the same site.

interpolated for each sample depth with no adjustment for the differences between mcd and rmcd. LSR was assigned to each sample using equation (1)

$$\mathrm{LSR}(i) = \frac{\mathrm{Depth}_{i+1} - \mathrm{Depth}_i}{\mathrm{Age}_{i+1} - \mathrm{Age}_i} \quad (1)$$

where i is the sample for which the LSR is calculated and $i+1$ is the next downhole sample. We use a 100 kyr smoothed LSR (Table S1) to avoid any abrupt changes in the instantaneous LSR based on the orbital time model. The DBD used are those from the ODP database which were based on direct measurement [*Mayer et al.*, 1992]. We stress that MAR estimates are only as accurate and detailed as the LSR estimates and the chronostratigraphy upon which they are based. Changes in DBD data are generally secondary in importance because, in absolute values, the variations in LSR are almost always greater than those in DBD. Sedimentation rates at this site are ~20–50 m Ma^{-1}. Dry bulk density (DBD) at this site has varied little, ranging between 0.63 and 0.77 g cm^{-3} throughout the Plio-Pleistocene [*Mayer et al.*, 1992].

For comparison and to ensure that postdeposition sediment redistribution (winnowing) is not heavily impacting our interpretation, BARs were also calculated using thorium-based MAR [*Winckler et al.*, 2008] and helium-based MAR [*Winckler et al.*, 2004] where data were available. Observed differences are small and do not change the conclusions of this paper (see Figures S1 and S2).

2.6. Export Production Calculation

BARs were used to reconstruct paleo-export production (g C m^{-2} yr^{-1}) using the relationship between BAR and export production derived from core top sediments according to *Eagle et al.* [2003] (see section 4.6 for details and supporting information for additional information). The original calibration was based on samples from the EEP collected at similar depths, providing credibility to the conversion.

3. Results

Both barite and carbonate content and accumulation rates at this site fluctuated considerably at multiple time scales (Figure 2). Barite and carbonate weight percent ranges from 200 to more than 6000 μg g^{-1} and from 50% to 90%, respectively, and accumulation rates range from less than 1 to over 10 mg cm^{-2} kyr^{-1} for barite and from less than 1 to over 3 g cm^{-2} kyr^{-1} for carbonate.

We compare temporal changes in export production derived from BAR over the past 4.3 Ma at site 849 to temperature trends in the area, including previously published records of (1) SST from nearby ODP site 847 [*Dekens et al.*, 2007], (2) subsurface temperatures at 849 [*Ford et al.*, 2012], and (3) the benthic oxygen isotopes record at 849 [*Mix et al.*, 1995] (Figure 3). Based on the long-term trends in export production, the record can be divided into three general periods: 4.3 to 3.0 Ma, 3.0 to 1.0 Ma, and 1.0 Ma to the present

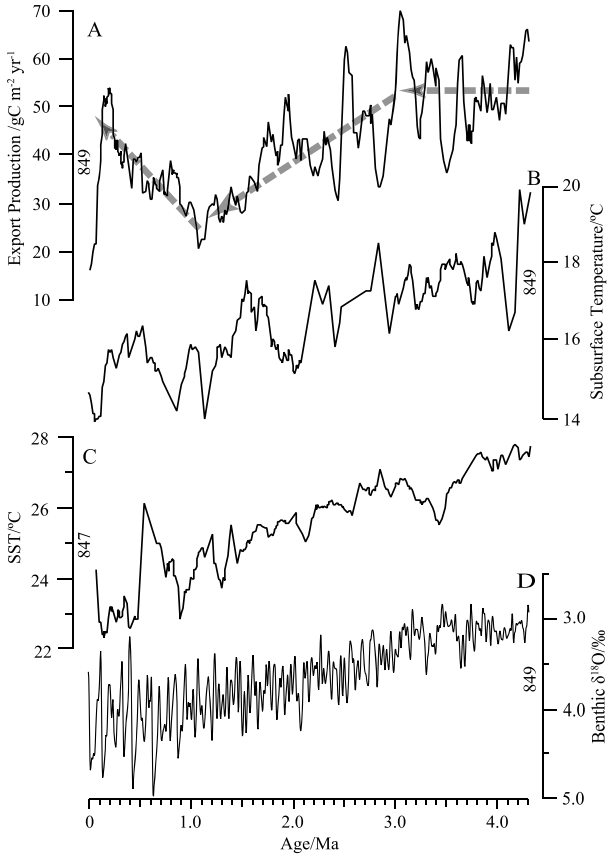

Figure 3. Ice volume, temperature, and export production in the EEP over the past 4.3 Ma. The figure shows changes in (a) export production with age over the past 4.3 Ma at site 849 along with (b) subsurface temperature at site 849 and (c) SST at site 847. (d) Oxygen isotope evolution of benthic foraminifera at site 849 (a proxy of ice volume) is also shown. All data except for benthic oxygen isotopes are 100 kyr smoothed values. Thermocline subsurface temperatures at site 849 are from *Ford et al.* [2012]; SSTs at site 847 based on alkenone unsaturation index are from *Dekens et al.* [2007], and benthic oxygen isotopes are from *Mix et al.* [1995].

(Figure 3a; also see Figure S3). These time segments correspond to other recorded changes in this region and to important climatic events as seen in the oxygen isotope record. Between 4.3 Ma and 3 Ma, export production was relatively high (average 51 g C m^{-2} yr^{-1}). Between 3 Ma and 1 Ma, a decrease in export production from 60 to 20 g C m^{-2} yr^{-1} is seen, while in the last million years, the trend reverses and export production generally increases (from 20 to 50 g C m^{-2} yr^{-1}), although there are high-amplitude variations. The export production over the entire 4.3 Ma record fluctuates between a maximum value of 110 g C m^{-2} yr^{-1} and a minimum value of 15 g C m^{-2} yr^{-1} (Figure 2d). Over the last 4.3 Ma, both SST and subsurface temperatures decrease; thus, the direction of change in the temperature and productivity records is not consistent throughout the record (Figure 3). The transitions in the trends in export production correspond to climatic events: at ~3 Ma the Northern Hemisphere glaciation (NHG) (3.6 to 2.4 Ma according to *Mudelsee and Raymo* [2005], with intensification of NHG at ~2.75 according to *Haug et al.* [1999]) and at ~1 Ma the mid-Pleistocene transition (MPT) (1.25 to 0.7 Ma and increase in ice volume around 1 Ma [*Elderfield et al.*, 2012; *Medina-Elizalde and Lea*, 2005]).

Higher fluctuations (up to five-fold) in BAR and hence export production are also seen in the record, and when our sampling resolution is high enough to resolve trends, these fluctuations seem to correspond to orbital frequencies (see Figure S4). These orbital-scale fluctuations in the record indicate that before 1.1 Ma, when 41 kyr variability of BAR and $\delta^{18}O$ dominate and the records are coherent, maxima in BARs occur at maxima in $\delta^{18}O$ (cold, glacial maxima) (Figures S4c, S4d, and 4). After 1.1 Ma, when 100 kyr variability dominates, the BAR maxima are offset from the $\delta^{18}O$ record (Figure S4d). This is particularly clear in the interval with the highest sampling resolution (between 120 and 340 kyr) (as shown in Figure 4).

4. Discussion

Productivity in the EEP has been very dynamic over the past 4.3 Ma. Export production rates, derived from BAR, have fluctuated considerably over this time interval. High-amplitude fluctuations of up to five-fold from 20 to 100 g C m^{-2} yr^{-1} (typically 2–2.5-fold) are seen in the record and are superimposed on long-term changes of the mean.

4.1. High Export Production Prior to Northern Hemisphere Glaciations

During the Late Pliocene, export productivity as calculated from BAR was on average quite high (~51 g C m^{-2} yr^{-1}) with peaks frequently reaching over 90 g C m^{-2} yr^{-1}. This period is also characterized by SST about 3–4°C higher than Late Pleistocene values [*Dekens et al.*, 2007; *Lawrence et al.*, 2006; *Wara et al.*, 2005] (Figure 3) and by subsurface temperatures that were also relatively warm [*Ford et al.*, 2012]. The high

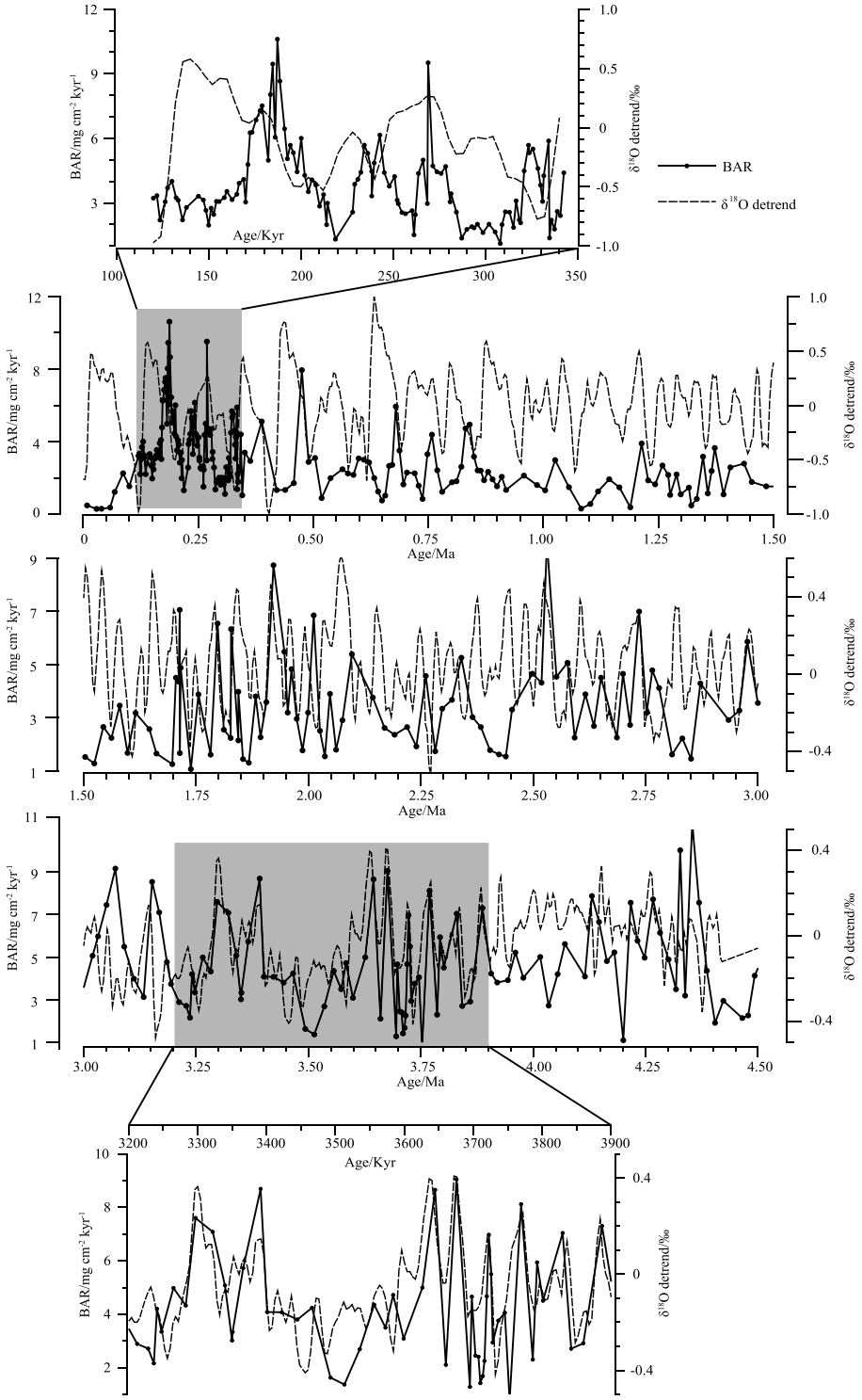

Figure 4. Plot of BAR (black line with dots) and detrended benthic oxygen isotope (thin dash line) at site 849 for the past 4.3 Ma. Note that for ease of comparison the oxygen isotope curves are plotted in reverse to convention (with high values on the top). Records between 120 kyr to 340 kyr and 3200 to 3900 kyr in the shaded area are expanded. High barite accumulation rates corresponding to heavy oxygen isotope values between 1.1 and 4.3 Ma suggest that high productivity occurred during glacial stages; after 1.1 Ma, accumulation rates are offset from the oxygen isotope changes, with maxima during deglacials. Benthic $\delta^{18}O$ are from *Mix et al.* [1995].

export production at this time suggests that, in the Late Pliocene, upwelling and atmospheric deposition-derived macronutrients and micronutrients were abundant and supported higher productivity than in the colder Pleistocene. This is consistent with the carbon isotope values of subsurface planktonic foraminifera which were relatively low, indicating high nutrient levels, during this period [*Cannariato and Ravelo*, 1997]. The surface to subsurface temperature gradient was not much different than at present, and there is no evidence for increased wind stress or changes in the position of the Intertropical Convergence Zone at that time [*Barreiro et al.*, 2006; *Haywood et al.*, 2007; *Hovan*, 1995; *Tziperman and Farrell*, 2009]. In fact, grain size data indicate that the wind speed at Site 849 remained roughly constant over the last 4.5 Ma [*Hovan*, 1995]; hence, it is expected that upwelling rates ($m^2\,s^{-1}$) were not higher than present. Accordingly, in order to support higher productivity, the upwelling water in the late Pliocene likely had higher macronutrient and micronutrient concentrations in comparison to the Pleistocene and to the present. Aeolian deposition of micronutrients like iron may have also been higher [*Hovan*, 1995], supporting increases in productivity.

The nutrient concentrations of upwelling waters are determined by the origin and age of the water mass and the degree and depth of local organic matter regeneration, while subsurface temperatures are primarily controlled by the temperatures at the location and time of the subsurface water mass formation. Our data therefore imply that the source of subsurface water in the Late Pliocene (warm and nutrient rich) was different than at present (cold and nutrient rich). Indeed, it has been suggested that during the Pliocene, prior to the Northern Hemisphere glaciations, temperatures were warmer at the extratropics South Pacific where the Equatorial Undercurrent (EUC) water originate [*Brierley et al.*, 2009; *Maslin et al.*, 1996]. This indicates that the entire upper ocean meridional overturning circulation in the Equatorial Pacific could have been considerably different than at present. Notably, warm temperatures increase overall metabolic rates, and if nutrients are plentiful, the higher temperatures may also contribute to enhanced productivity and to enhanced organic matter regeneration. In addition, all else being equal, warmer subsurface water can hold less CO_2 and when upwelled may be associated with a lower efflux of CO_2 to the atmosphere compared to colder water with the same nutrient content. Thus, during this time, warmer temperatures causing lower CO_2 efflux were countered by upwelling of more carbon/nutrient-enriched source water causing higher CO_2 efflux; hence, it is difficult to predict the net changes in CO_2 efflux. Specifically, our data alone cannot be used to reconstruct past pCO_2 in upwelled water, and proxies for carbonate system parameters such as B isotopes or B/Ca ratios would be useful for such inferences.

4.2. Decrease in EEP Export Production With the Intensification of NHG

From about 3 to 1 Ma, we observe a decrease in the mean export production from about 60 g C $m^{-2}\,yr^{-1}$ to less than 20 g C $m^{-2}\,yr^{-1}$ (Figure 3). This interval is also the time of declining SST and subsurface temperatures in the EEP as recorded by different temperature proxies [*Dekens et al.*, 2007; *Ford et al.*, 2012; *Ravelo et al.*, 2004; *Wara et al.*, 2005; *Lawrence et al.*, 2006] (Figure 3). In the modern ocean, on short timescales, an inverse relation between temperature and export production is seen, with periods of increased upwelling (like La Nina) showing high productivity associated with lower SST. This is not the relation seen in the trend between 3 and 1 Ma. While this decoupling between productivity (e.g., macronutrient and micronutrient input) and water temperature may seem paradoxical, we note that the processes that control temperature and nutrient distributions in the ocean are disparate and these parameters do not have to be coupled as they are at present.

Productivity in the EEP could have decreased as a result of (1) deepening of the nutricline (and thermocline) either by changes in the east-west tilt or in the average depth of the nutricline and thermocline, (2) declining upwelling rates resulting from lower wind stress, (3) lowering of the nutrient concentrations in upwelling water due to changes in chemistry of the source of the upwelled water, or (4) declining input of aeolian limiting micronutrients such as iron. The first possibility implies coupling between the thermocline and nutricline as in the present-day EEP, and in that case, lowering of SST should have resulted in a corresponding increase in productivity. However, as previously mentioned over this long (million year) time scale, the records between 3 and 1 Ma show the opposite relation. Thus, the first possibility is not consistent with the data, and indeed, published records suggest little change or even shoaling of the thermocline during this time period (Figure 3) [*Ford et al.*, 2012]. The second possibility, that decreasing wind-driven upwelling alone could explain the observed decreasing export production, is also unlikely because a decrease in upwelling is not consistent with the gradual SST cooling observed. Less upwelling would bring less cold thermocline water to the surface, which is inconsistent with the observed cooling trend. We can also eliminate the fourth

possibility since there is no clear indication based on grain size distribution in this core that the wind stress speed and associated aeolian deposition increased during this time interval [*Hovan*, 1995] and iron mass balance suggests that iron supply from dust and/or the Equatorial Undercurrent is not responsible for changes in export production in this region [*Ziegler et al.*, 2008]. Accordingly, we favor the third possibility, that the trend of decreasing export production in this area between 3 and 1 Ma is a result of a decrease in the nutrient content of the upwelled water resulting from an interoceanic reorganization of nutrient inventories (including iron).

Today, the cold, nutrient-rich waters of the ventilated thermocline upwelling in the EEP are sourced from intermediate and mode waters from the high latitudes of the North Pacific and the Southern Ocean [*Sarmiento et al.*, 2004; *Toggweiler et al.*, 1991; *Tsuchiya et al.*, 1989]. Climate changes and related changes in stratification, nutrient uptake, and productivity at these regions could result in changes in temperature and nutrient content of these source waters. Indeed, there is evidence that cooling and stratification in the polar source regions began at about 3 Ma [*Haug et al.*, 1999; *Martínez-Garcia et al.*, 2010; *Sigman et al.*, 2004]. The decrease in nutrient delivery in the EEP could therefore be related to an increase in productivity in the Antarctic Polar Front area which intensified around ~3 Ma as evidenced by biogenic silica deposition [*Cortese and Gersonde*, 2008]. This process would consume the nutrients (both macro and micro) before they are transported north toward the equator. Thus, we suggest that the decrease in productivity during this interval is related to a change in subsurface advective nutrient supply to the EEP (e.g., a colder nutrient poor water mass) and not to a change in upwelling rates.

The decrease in export productivity implies a decrease in the efficiency of the biological pump and less C sequestration. While we do not know if and how the CO_2 content of the upwelled water changed over this time interval, if nutrients and CO_2 content are correlated as they are in the present-day ocean, then the CO_2 efflux rate might have also decreased. Since the impact of lower C sequestration via the biological pump and lower CO_2 efflux have opposite effects on atmospheric CO_2, the net effect depends on the relative strength of these processes.

4.3. Export Production Increase Following the Mid-Pleistocene Transition

Continual cooling of the Northern Hemisphere over the past million years is characterized by the emergence and subsequent dominance of the large-amplitude, asymmetric quasi-100 kyr glacial-interglacial cycles [*McClymont et al.*, 2013]. At this time, a further decrease in SST, accompanied by a general increase in export production from an average of 20 g C m^{-2} yr^{-1} to about 50 g C m^{-2} yr^{-1} is seen at our site (Figure 3). These changes could be explained by increased wind stress and upwelling strength which would have lowered SST and increased nutrient availability to phytoplankton. However, the results could equally be explained by an increase in nutrient concentration and further cooling in source waters. Regolith erosion and weathering of the upper slope of marine sediments at high latitudes in response to falling sea level could have been the source of the nutrients that supported productivity during the middle Pleistocene transition as suggested by *Clark et al.* [2006]. This mechanism would imply a global increase in productivity, although currently not enough data exist to establish this. Increased aridity and associated atmospheric iron deposition [*Maher and Dennis*, 2001; *Wolff et al.*, 2006] may have also contributed to the increasing productivity at this time; which should similarly induce a global signal. However, the timing of maximum aeolian dust flux and export production is offset, so this is an unlikely explanation (see below). If indeed the higher productivity resulted from increased upwelling strength, CO_2 efflux may have also been higher, negating the increase in C sequestration by the biological pump. However, if the cause for this trend of increasing productivity is related to higher global ocean external nutrient input, then the increased productivity is expected to increase C sequestration via the biological pump, contributing to the cooling trend. To decipher which of the above mechanisms explains the trend observed over the past 1 Ma, export production should be reconstructed at diverse sites representing a variety of ecosystems and settings, particularly in areas not dominated by upwelling. Reconstruction of thermocline chemistry and specifically proxies that correspond to nutrient (Cd/Ca, $\delta^{13}C$) and carbonate system (B/Ca, $\delta^{11}B$) parameters could also aid in determining if the chemistry of upwelled water has changed, particularly if applied together with proxies of upwelling strength (e.g., Δ^{14}-$\delta^{13}C$, Ba/Ca).

Importantly, the relation between SST and export production over the last 1 Ma (SST cooling and increasing export production) is different than in the preceding 2 Ma between 3 and 1 Ma (SST cooling and decreasing export production), indicating that changes in SST and export production can be decoupled when

considering processes and trends that operate over million year time scales. Our data are most consistent with climate-induced changes in ocean circulation advecting waters with different nutrient contents to the EEP exerting the major control on these long-term trends. This is inconsistent with the interpretation of the continual decrease in SST and shoaling of the thermocline as an indication for the development of active upwelling cells (linked to wind cell intensification) in the EEP, provoking a net increase of primary productivity and an enhanced drawdown of atmospheric CO_2 in these regions [*Marlow et al.*, 2000]. While changes in export production and upwelling-related CO_2 efflux in the EEP could have potentially played a role in feedbacks between climate changes and the C cycle, records of changes in SST and BAR alone are not sufficient to arrive to that conclusion.

Our record of changes in mean export production as reconstructed from BAR over the past 4.3 Ma (long time scale) shows distinct shifts corresponding to changes in the cryosphere and climate. This suggests that global climate conditions have impacted local and global ocean circulation patterns responsible for nutrient delivery to the euphotic zone in this region.

4.4. Export Production Fluctuations on Orbital Time Scales

Unlike the long-term, million-year, time-scale trends, large-amplitude glacial-interglacial variations reveal synchronous and coupled changes in export production and the benthic oxygen isotope record, with higher BARs occurring during glacial periods (high $\delta^{18}O$) between 4.3 and 1.1 Ma. Although the sampling resolution of our record is ~10 kyr on average, which is too low in some intervals to visually correlate the $\delta^{18}O$ peaks with the BAR peaks; the length of the record allows us to resolve orbital-scale variability using a statistical treatment (Multi-Taper Method evolutive spectrum analysis, Figure S4) of the data. The analyses shows that the BAR record has spectral power in the 41 kyr and 100 kyr bands that is coherent at the 80% level with the benthic $\delta^{18}O$ record through much of the record. Coherency between $\delta^{18}O$ and export production (BAR) occurs in the obliquity band (41 kyr) from 4.3 to ~1.1 Ma and in the 100 kyr and 41 kyr bands in the most recent ~1.1 Ma (Figure S4).

From 4.3 to 1.1 Ma, high export production during glacials, observed in the 41 kyr band, is consistent with previous research in the EEP cold tongue, which indicates that alkenone productivity varied in phase with global ice volume changes at a dominant 41 kyr (obliquity) periodicity in the early Pliocene [*Lawrence et al.*, 2006]. This can be explained by intensified wind stress and upwelling during cold intervals, which enhanced the input of nutrients available for phytoplankton. However, changes in subsurface nutrient supply resulting from climate-induced changes in the region of source water formation cannot be ruled out. The two mechanisms are not mutually exclusive and may have operated in concert.

During and after the MPT (from ~1.1 Ma to the present), maximum export production typically lags maxima in the benthic $\delta^{18}O$ record (Figure S4d); thus, export production is relatively high during deglaciations and not during glacial maxima. In fact, export production rates are typically low during glacial maxima (Figure 4). A similar temporal lag is also recorded in the coccolithophore-related productivity records in the NW Pacific Ocean during the past 500 kyr [*Bordiga et al.*, 2014] and in biogenic opal accumulation records from the eastern and central equatorial Pacific [*Calvo et al.*, 2011; *Hayes et al.*, 2011]. This time period also coincides with a switch in the Pacific $CaCO_3$ dissolution cyclicity [*Sexton and Barker*, 2012] and in the $\delta^{13}C$-$\delta^{18}O$ correlation pattern in carbonates [*Turner*, 2014]. These data collectively suggest a fundamental change in the interplay between productivity and climate, associated with the intensification of the glaciation at the MPT.

The change in the dominant periodicity and phase relationship between export production and $\delta^{18}O$ at 1.1 Ma, around the time of the MPT, suggests a fundamental change in the relationship between nutrient supply and climate (glaciations and specifically ice volume). For example, prior to the MPT, it may be that wind strength controlled export productivity and simply responded directly to ice sheet size that modulated global temperature gradients. After the MPT, the lagged response of the export production to ice sheet size could indicate that nutrient cycling and circulation, and not simply upwelling strength, controlled export production. This is corroborated by the fact that SST variations lead alkenone production at a nearby EEP location [*Liu et al.*, 2008]. This increase could be related to a nutrient input pulse from exposed glacial flour, continental shelf, or other inputs that responded to glacial melt. Regardless of the exact mechanism associated with the observed changes in orbital variability and phase, it is noteworthy that there is, generally, a coupling between cooling climate and increasing export production in the EEP on orbital time scales. This is

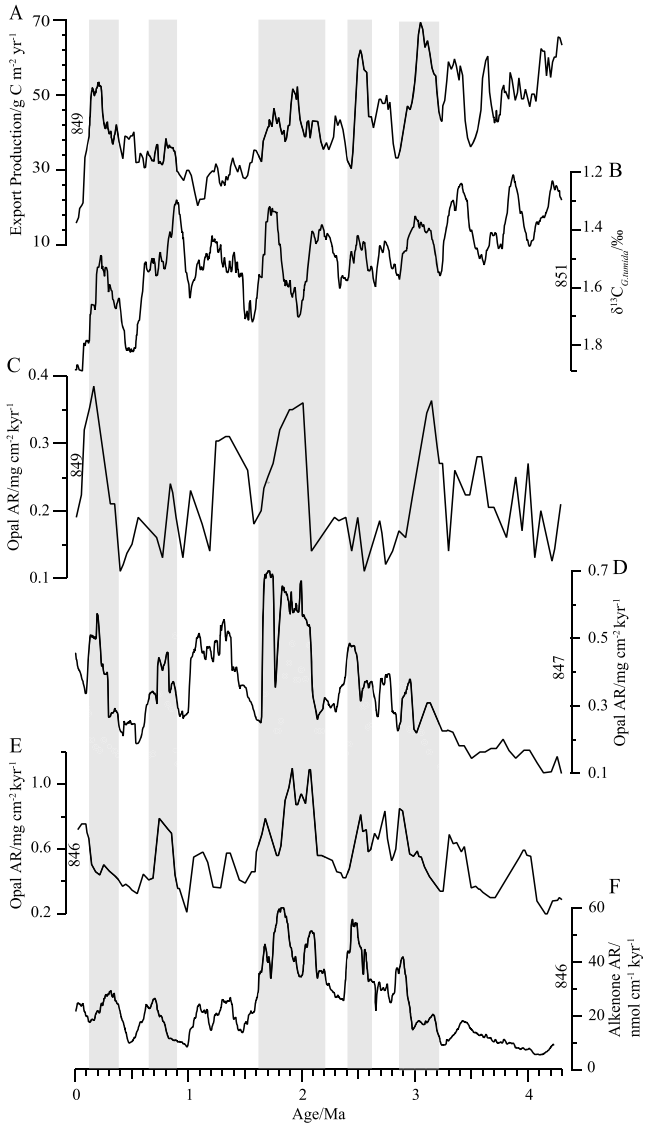

Figure 5. Comparison among productivity proxy records in the EEP over the past 4.3 Ma. (a) Barite-derived export production at site 849, (b) $\delta^{13}C$ *Globorotalia tumida* at site 851, (c) opal accumulation rates (ARs) at site 849, (d) opal AR at site 847, (e) opal AR at site 846, and (f) alkenone AR at site 846. $\delta^{13}C$ *G. tumida* for site 851 are from [*Cannariato and Ravelo*, 1997], opal ARs for sites 849, 847, and 846 are from *Farrell et al.* [1995] and alkenone ARs from *Lawrence et al.* [2006]. Note that all the data are treated with 100 kyr smooth.

in stark contrast to the general lack of coupling on long time (million years) scales, implying that different mechanisms drive changes in EEP export production on these two time scales.

4.5. Comparison With Other Published Productivity Records in the Region

When comparing our export production data to other published records of productivity for this region (Figures 5 and S5), we find some similarities but also some significant differences in temporal and spatial distributions. Specifically, the long-term (million years) export production trends seen at site 849 (e.g., high values at 4 Ma, a decrease from 3 to 1 Ma and an increase from 1 Ma on) differ considerably from trends in opal or alkenone accumulation further east at sites 846 and 847 (low values at 4 Ma increasing to a maximum at 2 Ma decreasing to 0.5 Ma and increasing thereafter). This spatial difference which has been observed in other records (e.g., records shown by *Lyle et al.* [1988] and *Mitchell* [1998]) emphasizes the impact of local circulation patterns in addition to global climate and tectonic forcing on productivity. The sites further to the east are affected by different water masses, specifically the Peru Current in addition to the EUC [*Farrell et al.*, 1995]. Moreover, these sites which are situated in the heart of the cold tongue record both coastal and equatorial upwelling, whereas 849 is more at the distal end recording mainly equatorial upwelling [*Pisias et al.*, 1995]. The differences observed in these trends are consistent with our suggestion that the long-term changes result from changes in circulation and the chemistry of the source waters and not from more global phenomena such as increased terrestrial nutrients input or intensification of wind stress. Interestingly, despite the divergence in the long-term trends, data from sites 846 [*Lawrence et al.*, 2006] and 847 [*Dekens et al.*, 2007] using alkenone, organic carbon, and bulk sediment accumulation rates also show decoupling between productivity and SST and call for upwelling of nutrient-enriched water when SSTs were warm in the early Pliocene [*Lawrence et al.*, 2006; *Mayer et al.*, 1992]. Similar to our reasoning in sections 4.1 and 4.2, this decoupling between productivity and SST is also consistent with temporal and spatial changes in circulation patterns impacting ocean productivity in this region. Specifically, at site 849 between 4 and 2 Ma, the upwelled water became colder and lower in nutrients, a pattern also consistent with the increase in $\delta^{13}C$ of *Globorotalia tumida* at Site 851 which is close to 849 (Figure 5b), while to the east of these sites, the nutrient content increased along with the cooling, possibly implying the existence of a water mass that is unique to the more eastern part of the equatorial Pacific.

It is also possible that differences between BAR at 849 and opal accumulation at 846 and 847 arise because barite and opal are recording different components of ocean productivity (export production and diatom productivity, respectively) and these were decoupled, as discussed by *Pisias et al.* [1995] and *Ma et al.* [2014]. This however would require that, in the Pliocene for example, diatom productivity was low (low opal) but export production high (high BAR) while oceanographic observations suggest that in fact relatively high particulate organic carbon export is typically associated with diatoms [*Buesseler*, 1998]. Differences in opal preservation over time (e.g., less preservation in the Pliocene) can also cause disparate trends in the BAR and opal records. However, the trends in opal are also seen in alkenone accumulation as well as total nitrogen and organic matter at the eastern sites [*Buesseler*, 1998], and there is no reason to assume that preservation for all of these proxies will change in the same manner. Moreover, the pattern of opal accumulation at site 849 (Figure 5c) also differs from the opal trends at 847 and 846 (Figures 5d and 5e), suggesting that the differences are not artifacts of comparing different proxies or are a result of differences in preservation (sites are at similar depths) but rather reflect real spatial differences resulting from impacts of distinct water masses at these sites. It is interesting that the absolute values of opal MAR are almost the same at 849, 847, and 846 around 4 Ma, suggesting that in the early Pliocene opal MAR was relatively uniform throughout the EEP. Then, as the cold tongue productivity increased between 4 and 2 Ma, the modern pattern of opal MAR developed with higher values close to 846 and 847 compared to 849.

Although our data are indicative of differences in the water masses that feed upwelling at 849 and at 847/846, it is also conceivable that in addition to changes in source water there are differences in upwelling strength among the sites. The increase in productivity and decrease in SST at 847/846 may suggest an increase in the upwelling strength between 4 and 2 Ma, which did not impact site 849. A change in the northerly component of the trades (e.g., a slight cooling of the cold tongue resulting in increased N-S SST gradient between the eastern warm pool and the cold tongue and leading to enhanced northerly winds), which drove changes in Peru coastal upwelling and cold tongue nutrients will have less of an impact at site 849 compared to 847/846.

Another observation is that on the long time scale, trends based on different productivity proxies do not always agree. For example, at 849, BAR has a general decreasing trend from 3 to 1 Ma, whereas in the same site (849), the opal MAR does not have a pronounced decreasing trend, and neither does the organic C signal [*Farrell et al.*, 1995]. It is possible that the opal and organic C concentrations in this core are too low to capture the trend. Moreover, the data are of very low resolution and there is a lot of variability [*Farrell et al.*, 1995], so it is possible that the available data are not sufficient to capture the trends. Alternatively, as previously noted, different proxies are impacted by additional factors; it is possible that both opal and organic C are poorly preserved in this deep setting while barite is less susceptible to dissolution and thus may better reflect export production at this site, or that export production was not dominated by diatom and coccolithophore productivity. One other possibility is that, as subsurface temperatures cool, the rates of organic matter mineralization (degradation) by bacteria decrease, resulting in lower barite formation [*Ma et al.*, 2014] and decoupling between surface water productivity (carbonate and opal production) and export production (BAR). However, if this is an important process that is dominating the record, it would have been expected that in the last part of the record from 1 Ma to the present, as temperatures continue to cool, BAR would continue to decrease, which is not the case. Moreover, the barite export production core top calibration curve is based on samples from the Southern Ocean to the equatorial Atlantic, spanning a range of temperatures which are included in the empirical relation. The impact of temperature on barite formation in the ocean should further be investigated to yield a quantitative relation.

On shorter time scales, there is better correspondence among the various productivity proxies. For example, most of the records in Figure 5 (including BAR) show three time intervals with relatively high productivity and export production: between 2800 and 2500 kyr, 2200 and 1600 kyr, and 250 and 100 kyr (Figure 5, gray bars). This is superimposed on the long-term trends. The various proxies record different components of ocean productivity; opal and alkenone accumulation rates represent the abundance of diatoms and haptophyte algae, respectively, while BARs record the regeneration of sinking organic matter below the euphotic zone and organic C and N accumulations represent the burial in the sediment. The correspondence between these various proxies suggests that export production and organic matter burial were proportional to the net productivity of these specific major phytoplankton groups, at least during these specific time intervals in this region, a situation similar to that in the present day.

Our data for the orbital time-scale fluctuations (glacial-interglacial) are also consistent with most previously published records. Particularly, *Lawrence et al.* [2006] and *Liu and Herbert* [2004] observed, in the early Pliocene, that higher alkenone concentrations almost universally occurred during cold intervals, indicating that temperature and productivity were tightly coupled on orbital time scales ($<10^5$ years) in the Plio-Pleistocene. Similar trends were also observed in other paleoproductivity proxies [*Bolton et al.*, 2010a, 2010b; *Lyle et al.*, 1988; *Paytan et al.*, 1996; *Pedersen*, 1983; *Pedersen et al.*, 1991; *Pichat et al.*, 2004; *Sarnthein et al.*, 1988, and references therein] and are generally consistent with intensification of upwelling during cold intervals that fuel surface productivity (prior to ~1.1 Ma). Increased dust deposition during glacial times [*Fuhrer et al.*, 1993; *Hovan*, 1995; *Petit et al.*, 1999] could have also contributed to the higher productivity seen prior to 1.1 Ma.

The observed shift in the timing of maximum export production relative to climate parameters (e.g., $\delta^{18}O$, ice volume, SST, and dust deposition) at ~1.1 Ma which is also captured in other records in this region, including opal accumulation and diatom biomarkers [*Hayes et al.*, 2011], C isotopes [*Lisiecki*, 2010; *Turner*, 2014], and N isotopes [*Robinson et al.*, 2009] indicates a change in this coupling. In relation to drivers, it is interesting to note that records of dust deposition as seen in ice cores [*Fuhrer et al.*, 1993; *Petit et al.*, 1999] and in sedimentary records in this region [*Anderson et al.*, 2006; *Calvo et al.*, 2011; *McGee et al.*, 2007; *Winckler et al.*, 2008] are highest during maximum glaciations while the maximum productivity is offset from glacial maxima (mostly during deglaciation), suggesting that dust deposition did not contribute to increased productivity in the EEP since 1.1 Ma. There are several processes that may have contributed to increased productivity during deglacials; either the poleward movement of the westerlies and retreat of sea ice increased upwelling and enriched surface waters in the south Pacific, which is the source of water to the EEP, and/or there could have been new nutrient inputs from weathering of continental shelf and freshly exposed glacial flour.

5. Summary and Conclusions

Our results indicate that different mechanisms may drive changes in EEP surface conditions on different time scales. On long time scales, changes are primarily controlled by changes in nutrient content of water masses that contribute to the subsurface water upwelling in the EEP; climate-induced circulation change might play a dominant role on the long-time-scale variations. In the Late Pliocene at our site, both productivity and SST were high, indicative of upwelling of warm nutrient-rich water in the region. With the initiation of Northern Hemisphere glaciation at ~3 Ma, a gradual concurrent decrease in SST and productivity in the EEP indicates cooling and depletion in nutrients of source waters to this area. This trend changed about 1 Ma ago, showing an increase in productivity while SSTs continue to decrease. These long-term trends differ at different locations within the EEP, indicating regional variability in circulation and water masses.

On shorter time scales between 4.3 and 1.1 Ma, export production was more intense during glacials, likely a result of the increase in wind-driven upwelling and possibly also dust deposition. Starting at ~1.1 Ma, the amplitude of export productivity changes intensified and the export production maxima shifted from coinciding with glacial maxima to sharp peaks at the transitions between glacials and interglacials (deglacials), indicative of changes in nutrient content of upwelled water.

The changes in marine export production and upwelling-associated CO_2 efflux may have played a role in the global carbon cycle and could have had an influence on climatic change providing internal climate feedbacks through the modification of atmospheric CO_2 levels. Proxies specific to upwelling rate and carbonate system chemistry in upwelling water are needed to determine the direction and magnitude of these feedbacks. Most importantly, if we are to understand the role of the tropics in modulating climate change, it would be useful if models could reproduce the distinct changes in EEP export production, their amplitude, initiation and termination in relation to ice volume, temperature, and circulation changes on both the long-term and orbital time scales over the last 4.3 Ma.

Acknowledgments

Z. Ma was supported by the NSFC (grant 41406053). This study was also partly supported by 111 project (B14001) of Ministry of Education, China. This work was funded by NSF CAREER grant OCE-0449732 to A.P. All the data for this paper are presented in Table S1 and will be deposited in the Pangaea Data Repository (http://www.pangaea.de/) or can be requested directly from the corresponding author (apaytan@ucsc.edu).

References

Anderson, R., M. Fleisher, and Y. Lao (2006), Glacial-interglacial variability in the delivery of dust to the central equatorial Pacific Ocean, *Earth Planet. Sci. Lett.*, *242*(3), 406–414, doi:10.1016/j.epsl.2005.11.061.

Barreiro, M., G. Philander, R. Pacanowski, and A. Fedorov (2006), Simulations of warm tropical conditions with application to middle Pliocene atmospheres, *Clim. Dyn.*, *26*(4), 349–365, doi:10.1007/s00382-005-0086-4.

Bjerknes, J. (1969), Atmospheric teleconnections from the equatorial Pacific, *Mon. Weather Rev.*, *97*(3), 163–172, doi:10.1175/1520-0493(1969)097<0163:atftep>2.3.co;2.

Bolton, C. T., S. J. Gibbs, and P. A. Wilson (2010a), Evolution of nutricline dynamics in the equatorial Pacific during the late Pliocene, *Paleoceanography*, *25*, PA1207, doi:10.1029/2009PA001821.

Bolton, C. T., K. T. Lawrence, S. J. Gibbs, P. A. Wilson, L. C. Cleaveland, and T. D. Herbert (2010b), Glacial-interglacial productivity changes recorded by alkenones and microfossils in late Pliocene eastern equatorial Pacific and Atlantic upwelling zones, *Earth Planet. Sci. Lett.*, *295*(3–4), 401–411, doi:10.1016/j.epsl.2010.04.014.

Bordiga, M., M. Cobianchi, C. Lupi, N. Pelosi, N. L. Venti, and P. Ziveri (2014), Coccolithophore carbonate during the last 450 ka in the NW Pacific Ocean (ODP site 1209B, Shatsky Rise), *J. Quat. Sci.*, *29*(1), 57–69, doi:10.1002/jqs.2677.

Brierley, C. M., A. V. Fedorov, Z. Liu, T. D. Herbert, K. T. Lawrence, and J. P. LaRiviere (2009), Greatly expanded tropical warm pool and weakened Hadley circulation in the early Pliocene, *Science*, *323*(5922), 1714–1718, doi:10.1126/science.1167625.

Bryden, H. L., and E. C. Brady (1985), Diagnostic model of the three-dimensional circulation in the upper equatorial Pacific Ocean, *J. Phys. Oceanogr.*, *15*(10), 1255–1273, doi:10.1175/1520-0485(1985)015<1255:DMOTTD>2.0.CO;2.

Buesseler, K. O. (1998), The decoupling of production and particulate export in the surface ocean, *Global Biogeochem. Cycles*, *12*(2), 297–310, doi:10.1029/97GB03366.

Calvo, E., C. Pelejero, L. D. Pena, I. Cacho, and G. A. Logan (2011), Eastern equatorial Pacific productivity and related-CO_2 changes since the last glacial period, *Proc. Natl. Acad. Sci. U.S.A.*, *108*(14), 5537–5541, doi:10.1073/pnas.1009761108.

Cane, M. A. (1998), Climate change: A role for the tropical Pacific, *Science*, *282*(5386), 59–61, doi:10.1126/science.282.5386.59.

Cane, M. A. (2005), The evolution of El Niño, past and future, *Earth Planet. Sci. Lett.*, *230*(3–4), 227–240, doi:10.1016/j.epsl.2004.12.003.

Cannariato, K. G., and A. C. Ravelo (1997), Pliocene-Pleistocene evolution of eastern tropical Pacific surface water circulation and thermocline depth, *Paleoceanography*, *12*(6), 805–820, doi:10.1029/97PA02514.

Chavez, F. P., and R. T. Barber (1987), An estimate of new production in the equatorial Pacific, *Deep-Sea Res., Part A*, *34*(7), 1229–1243, doi:10.1016/0198-0149(87)90073-2.

Clark, P. U., D. Archer, D. Pollard, J. D. Blum, J. A. Rial, V. Brovkin, A. C. Mix, N. G. Pisias, and M. Roy (2006), The middle Pleistocene transition: Characteristics, mechanisms, and implications for long-term changes in atmospheric pCO_2, *Quat. Sci. Rev.*, *25*(23–24), 3150–3184, doi:10.1016/j.quascirev.2006.07.008.

Cortese, G., and R. Gersonde (2008), Plio/Pleistocene changes in the main biogenic silica carrier in the Southern Ocean, Atlantic Sector, *Mar. Geol.*, *252*(3–4), 100–110, doi:10.1016/j.margeo.2008.03.015.

Cox, P. M., R. A. Betts, C. D. Jones, S. A. Spall, and I. J. Totterdell (2000), Acceleration of global warming due to carbon-cycle feedbacks in a coupled climate model, *Nature*, *408*(6809), 184–187, doi:10.1038/35041539.

Dekens, P. S., A. C. Ravelo, and M. D. McCarthy (2007), Warm upwelling regions in the Pliocene warm period, *Paleoceanography*, *22*, PA3211, doi:10.1029/2006PA001394.

Diester-Haass, L., K. Billups, and K. C. Emeis (2006), Late Miocene carbon isotope records and marine biological productivity: Was there a (dusty) link?, *Paleoceanography*, *21*, PA4216, doi:10.1029/2006PA001267.

Eagle, M., A. Paytan, K. R. Arrigo, G. van Dijken, and R. W. Murray (2003), A comparison between excess barium and barite as indicators of carbon export, *Paleoceanography*, *18*(1), 1021, doi:10.1029/2002PA000793.

Elderfield, H., P. Ferretti, M. Greaves, S. Crowhurst, I. McCave, D. Hodell, and A. Piotrowski (2012), Evolution of ocean temperature and ice volume through the mid-Pleistocene climate transition, *Science*, *337*(6095), 704–709, doi:10.1126/science.1221294.

Etourneau, J., R. S. Robinson, P. Martinez, and R. Schneider (2013), Equatorial Pacific peak in biological production regulated by nutrient and upwelling during the late Pliocene/early Pleistocene cooling, *Biogeosciences*, *10*(8), 5663–5670, doi:10.5194/bg-10-5663-2013.

Falkowski, P., E. Laws, R. Barber, and J. Murray (2003), Phytoplankton and their role in primary, new, and export production, in *Ocean Biogeochemistry*, edited by M. R. Fasham, pp. 99–121, Springer, Berlin, doi:10.1007/978-3-642-55844-3_5.

Falkowski, P. G., R. T. Barber, and V. Smetacek (1998), Biogeochemical controls and feedbacks on ocean primary production, *Science*, *281*(5374), 200–206, doi:10.1126/science.281.5374.200.

Farrell, J. W., I. Raffi, T. R. Janecek, D. W. Murray, M. Levitan, K. A. Dadey, K.-C. Emeis, M. Lyle, J.-A. Flores, and S. Hovan (1995), Late Neogene sedimentation patterns in the eastern equatorial Pacific Ocean, *Proc. Ocean Drill. Program: Sci. Results*, *138*, 717–756, doi:10.2973/odp.proc.sr.138.143.1995.

Fedorov, A. V., C. M. Brierley, and K. Emanuel (2010), Tropical cyclones and permanent El Niño in the early Pliocene epoch, *Nature*, *463*(7284), 1066–1070, doi:10.1038/nature08831.

Fiedler, P. C., V. Philbrick, and F. P. Chavez (1991), Oceanic upwelling and productivity in the Eastern Tropical Pacific, *Limnol. Oceanogr.*, *36*(8), 1834–1850.

Ford, H. L., A. C. Ravelo, and S. Hovan (2012), A deep eastern equatorial Pacific thermocline during the early Pliocene warm period, *Earth Planet. Sci. Lett.*, *355–356*, 152–161, doi:10.1016/j.epsl.2012.08.027.

Fuhrer, K., A. Neftel, M. Anklin, and V. Maggi (1993), Continuous measurements of hydrogen peroxide, formaldehyde, calcium and ammonium concentrations along the new grip ice core from summit, Central Greenland, *Atmos. Environ., Part A*, *27*(12), 1873–1880, doi:10.1016/0960-1686(93)90292-7.

Gartner, S., J. Chow, and R. J. Stanton Jr. (1987), Late Neogene paleoceanography of the eastern Caribbean, the Gulf of Mexico, and the eastern Equatorial Pacific, *Mar. Micropaleontol.*, *12*, 255–304, doi:10.1016/0377-8398(87)90024-7.

Gonneea, M. E., and A. Paytan (2006), Phase associations of barium in marine sediments, *Mar. Chem.*, *100*(1–2), 124–135, doi:10.1016/j.marchem.2005.12.003.

Hagelberg, T. K., N. G. Pisias, N. J. Shackleton, A. C. Mix, and S. Harris (1995), Refinement of a high-resolution, continuous sedimentary section for studying equatorial Pacific Ocean paleoceanography, *Proc. Ocean Drill. Program: Sci. Results*, *138*, 31–46, doi:10.2973/odp.proc.sr.138.103.1995.

Haug, G. H., D. M. Sigman, R. Tiedemann, T. F. Pedersen, and M. Sarnthein (1999), Onset of permanent stratification in the subarctic Pacific Ocean, *Nature*, *401*(6755), 779–782, doi:10.1038/44550.

Hayes, C. T., R. F. Anderson, and M. Q. Fleisher (2011), Opal accumulation rates in the equatorial Pacific and mechanisms of deglaciation, *Paleoceanography*, *26*, PA1207, doi:10.1029/2010PA002008.

Haywood, A. M., and P. J. Valdes (2004), Modelling Pliocene warmth: Contribution of atmosphere, oceans and cryosphere, *Earth Planet. Sci. Lett.*, *218*(3–4), 363–377, doi:10.1016/S0012-821X(03)00685-X.

Haywood, A. M., P. J. Valdes, and V. L. Peck (2007), A permanent El Niño-like state during the Pliocene?, *Paleoceanography*, *22*, PA1213, doi:10.1029/2006PA001323.

Haywood, A. M., H. J. Dowsett, M. M. Robinson, D. K. Stoll, A. M. Dolan, D. J. Lunt, B. Otto-Bliesner, and M. A. Chandler (2011), Pliocene Model Intercomparison Project (PlioMIP): Experimental design and boundary conditions (experiment 2), *Geosci. Model Dev.*, *4*(3), 571–577, doi:10.5194/gmd-4-571-2011.

Hovan, S. (1995), Late Cenozoic atmospheric circulation intensity and climatic history recorded by Eolian deposition in the Eastern Equatorial Pacific Ocean, Leg 138, *Proc. Ocean Drill. Program: Sci. Results*, *138*, 615–625, doi:10.2973/odp.proc.sr.138.132.1995.

Jickells, T. D., et al. (2005), Global iron connections between desert dust, ocean biogeochemistry, and climate, *Science*, *308*(5718), 67–71, doi:10.1126/science.1105959.

Kemp, A. E. S. (1995), Neogene and Quaternary pelagic sediments and depositional history of the eastern equatorial Pacific Ocean (Leg 138), *Proc. Ocean Drill. Program: Sci. Results*, *138*, 627–639, doi:10.2973/odp.proc.sr.138.133.1995.

King, S. C., J. W. Murray, and A. E. S. Kemp (1998), Palaeoenvironments of deposition of Neogene laminated diatom mat deposits from the eastern equatorial Pacific from studies of benthic foraminifera (sites 844, 849, 851), *Mar. Micropaleontol.*, *35*(3–4), 161–177, doi:10.1016/S0377-8398(98)00020-6.

Lawrence, K. T., Z. Liu, and T. D. Herbert (2006), Evolution of the eastern tropical Pacific through Plio-Pleistocene glaciation, *Science*, *312*(5770), 79–83, doi:10.1126/science.1120395.

Lisiecki, L. E. (2010), A benthic δ^{13}C-based proxy for atmospheric pCO_2 over the last 1.5 Myr, *Geophys. Res. Lett.*, *37*, L21708, doi:10.1029/2010GL045109.

Liu, Z., and T. D. Herbert (2004), High-latitude influence on the eastern equatorial Pacific climate in the early Pleistocene epoch, *Nature*, *427*(6976), 720–723, doi:10.1038/nature02338.

Liu, Z., L. C. Cleaveland, and T. D. Herbert (2008), Early onset and origin of 100-kyr cycles in Pleistocene tropical SST records, *Earth Planet. Sci. Lett.*, *265*(3–4), 703–715, doi:10.1016/j.epsl.2007.11.016.

Loubere, P. (2000), Marine control of biological production in the eastern equatorial Pacific Ocean, *Nature*, *406*, 497–500, doi:10.1038/35020041.

Lyle, M., D. W. Murray, B. P. Finney, J. Dymond, J. M. Robbins, and K. Brooksforce (1988), The record of late Pleistocene biogenic sedimentation in the Eastern Tropical Pacific Ocean, *Paleoceanography*, *3*(1), 39–59, doi:10.1029/PA003i001p00039.

Ma, Z., E. Gray, E. Thomas, B. Murphy, J. Zachos, and A. Paytan (2014), Carbon sequestration during the Palaeocene-Eocene thermal maximum by an efficient biological pump, *Nat. Geosci.*, *7*(5), 382–388, doi:10.1038/ngeo2139.

Maher, B. A., and P. F. Dennis (2001), Evidence against dust-mediated control of glacial-interglacial changes in atmospheric CO_2, *Nature*, *411*(6834), 176–180, doi:10.1038/35075543.

Markovic, S., A. Paytan, and U. G. Wortmann (2015), Pleistocene sediment offloading and the global sulfur cycle, *Biogeosciences*, *12*(10), 3043–3060, doi:10.5194/bg-12-3043-2015.

Marlow, J. R., C. B. Lange, G. Wefer, and A. Rosell-Mele (2000), Upwelling intensification as part of the Pliocene-Pleistocene climate transition, *Science*, *290*(5500), 2288–2291, doi:10.1126/science.290.5500.2288.

Martínez-Garcia, A., A. Rosell-Melé, E. L. McClymont, R. Gersonde, and G. H. Haug (2010), Subpolar link to the emergence of the modern equatorial pacific cold tongue, *Science*, *328*(5985), 1550–1553, doi:10.1126/science.1184480.

Maslin, M., G. Haug, M. Sarnthein, and R. Tiedemann (1996), The progressive intensification of Northern Hemisphere glaciation as seen from the North Pacific, *Geol. Rundsch.*, *85*(3), 452–465, doi:10.1007/bf02369002.

Matsumoto, K., T. Oba, J. Lynch-Stieglitz, and H. Yamamoto (2002), Interior hydrography and circulation of the glacial Pacific Ocean, *Quat. Sci. Rev.*, *21*(14–15), 1693–1704, doi:10.1016/S0277-3791(01)00142-1.

Mayer, L., F. Theyer, J. A. Barron, D. A. Dunn, T. Handyside, and S. Hills (Eds.) (1985), *Initial Reports: DSDP 85*, U.S. Govt. Printing Office, Washington, doi:10.2973/dsdp.proc.85.1985.

Mayer, L., N. Pisias, and T. Janecek (Eds.) (1992), *Proceedings of the Ocean Drilling Program, Initial Reports*, vol. 138, Ocean Drilling Program, College Station, Tex., doi:10.2973/odp.proc.ir.138.1992.

McClymont, E. L., S. M. Sosdian, A. Rosell-Melé, and Y. Rosenthal (2013), Pleistocene sea-surface temperature evolution: Early cooling, delayed glacial intensification, and implications for the mid-Pleistocene climate transition, *Earth Sci. Rev.*, *123*, 173–193. doi:10.1016/j.earscirev.2013.04.006

McGee, D., F. Marcantonio, and J. Lynch-Stieglitz (2007), Deglacial changes in dust flux in the eastern equatorial Pacific, *Earth Planet. Sci. Lett.*, *257*(1–2), 215–230, doi:10.1016/j.epsl.2007.02.033.

Medina-Elizalde, M., and D. W. Lea (2005), The mid-Pleistocene transition in the Tropical Pacific, *Science*, *310*(5750), 1009–1012, doi:10.1126/science.1115933.

Mitchell, N. C. (1998), Sediment accumulation rates from Deep Tow profiler records and DSDP Leg 70 cores over the Galapagos spreading centre, *Geol. Soc. London, Spec. Publ.*, *131*(1), 199–209, doi:10.1144/gsl.sp.1998.131.01.13.

Mix, A. C., N. G. Pisias, W. Rugh, J. Wilson, A. Morey, and T. K. Hagelber (1995), Benthic foraminifer stable isotope record from Site 849 (0–5 Ma): Local and global climate changes, *Proc. Ocean Drill. Program: Sci. Results*, *138*, 371–412, doi:10.2973/odp.proc.sr.138.120.1995.

Mix, A. C., et al. (Eds.) (2003), *Proceedings of the Ocean Drilling Program: Initial Reports*, Ocean Drill. Program, College Station, Tex., doi:10.2973/odp.proc.ir.202.2003.

Mudelsee, M., and M. E. Raymo (2005), Slow dynamics of the Northern Hemisphere glaciation, *Paleoceanography*, *20*, PA4022, doi:10.1029/2005PA001153.

Pagani, M., Z. Liu, J. LaRiviere, and A. C. Ravelo (2010), High Earth-system climate sensitivity determined from Pliocene carbon dioxide concentrations, *Nat. Geosci.*, *3*(1), 27–30, doi:10.1038/ngeo724.

Paytan, A. (2009), Ocean paleoproductivity, in *Encyclopedia of Paleoclimatology and Ancient Environments*, edited by V. Gornitz, pp. 644–651, Springer, Netherlands, doi:10.1007/978-1-4020-4411-3_158.

Paytan, A., and E. M. Griffith (2007), Marine Barite: Recorder of variations in ocean export productivity, *Deep Sea Res., Part II*, 687–705, doi:10.1016/j.dsr2.2007.01.007.

Paytan, A., M. Kastner, and F. P. Chavez (1996), Glacial to interglacial fluctuations in productivity in the equatorial Pacific as indicated by marine barite, *Science*, *274*(5291), 1355–1357, doi:10.1126/science.274.5291.1355.

Pedersen, T. F. (1983), Increased productivity in the eastern equatorial Pacific during the Last Glacial Maximum (19,000 to 14,000 yr B.P.), *Geology*, *11*(1), 16–19, doi:10.1130/0091-7613(1983)11<16:ipitee>2.0.co;2.

Pedersen, T. F., B. Nielsen, and M. Pickering (1991), Timing of Late Quaternary productivity pulses in the Panama Basin and implications for atmospheric CO_2, *Paleoceanography*, *6*(6), 657–677, doi:10.1029/91PA02532.

Pennington, J. T., K. L. Mahoney, V. S. Kuwahara, D. D. Kolber, R. Calienes, and F. P. Chavez (2006), Primary production in the eastern tropical Pacific: A review, *Prog. Oceanogr.*, *69*(2–4), 285–317, doi:10.1016/j.pocean.2006.03.012.

Petit, J. R., et al. (1999), Climate and atmospheric history of the past 420,000 years from the Vostok ice core, Antarctica, *Nature*, *399*(6735), 429–436, doi:10.1038/20859.

Pichat, S., K. W. W. Sims, R. François, J. F. McManus, S. Brown Leger, and F. Albarède (2004), Lower export production during glacial periods in the equatorial Pacific derived from $(^{231}Pa/^{230}Th)_{xs,0}$ measurements in deep-sea sediments, *Paleoceanography*, *19*, PA4023, doi:10.1029/2003PA000994.

Pisias, N. G., L. A. Mayer, and A. C. Mix (1995), Paleoceanography of the eastern equatorial Pacific during the Neogene: Synthesis of Leg 138 drilling results, *Proc. Ocean Drill. Program: Sci. Results*, *138*, 5–21, doi:10.2973/odp.proc.sr.138.101.1995.

Ravelo, A. C., D. H. Andreasen, M. Lyle, A. Olivarez Lyle, and M. W. Wara (2004), Regional climate shifts caused by gradual global cooling in the Pliocene epoch, *Nature*, *429*(6989), 263–267, doi:10.1038/nature02567.

Robinson, R. S., P. Martinez, L. D. Pena, and I. Cacho (2009), Nitrogen isotopic evidence for deglacial changes in nutrient supply in the eastern equatorial Pacific, *Paleoceanography*, *24*, PA4213, doi:10.1029/2008PA001702.

Sarmiento, J. L., N. Gruber, M. A. Brzezinski, and J. P. Dunne (2004), High-latitude controls of thermocline nutrients and low latitude biological productivity, *Nature*, *427*(6969), 56–60, doi:10.1038/nature02127.

Sarnthein, M., K. Winn, J.-C. Duplessy, and M. R. Fontugne (1988), Global variations of surface ocean productivity in low and mid latitudes: Influence on CO_2 reservoirs of the deep ocean and atmosphere during the last 21,000 years, *Paleoceanography*, *3*(3), 361–399, doi:10.1029/PA003i003p00361.

Schneider, B., and A. Schmittner (2006), Simulating the impact of the Panamanian seaway closure on ocean circulation, marine productivity and nutrient cycling, *Earth Planet. Sci. Lett.*, *246*(3–4), 367–380, doi:10.1016/j.epsl.2006.04.028.

Schneider, B., L. Bopp, M. Gehlen, J. Segschneider, T. Frölicher, P. Cadule, P. Friedlingstein, S. Doney, M. Behrenfeld, and F. Joos (2008), Climate-induced interannual variability of marine primary and export production in three global coupled climate carbon cycle models, *Biogeosciences*, *5*, 597–614, doi:10.5194/bg-5-597-2008.

Seki, O., G. L. Foster, D. N. Schmidt, A. Mackensen, K. Kawamura, and R. D. Pancost (2010), Alkenone and boron-based Pliocene pCO_2 records, *Earth Planet. Sci. Lett.*, *292*(1–2), 201–211, doi:10.1016/j.epsl.2010.01.037.

Sexton, P. F., and S. Barker (2012), Onset of 'Pacific-style' deep-sea sedimentary carbonate cycles at the mid-Pleistocene transition, *Earth Planet. Sci. Lett.*, *321–322*, 81–94, doi:10.1016/j.epsl.2011.12.043.

Shackleton, N. J., S. Crowhurst, T. Hagelberg, N. G. Pisias, and D. A. Schneider (1995), A new late Neogene time scale: Application to Leg 138 sites, *Proc. Ocean Drill. Program: Sci. Results*, *138*, 73–101, doi:10.2973/odp.proc.sr.138.106.1995.

Sigman, D. M., S. L. Jaccard, and G. H. Haug (2004), Polar ocean stratification in a cold climate, *Nature*, *428*(6978), 59–63, doi:10.1038/nature02357.

Steph, S., R. Tiedemann, J. Groeneveld, A. Sturm, and D. Nürnberg (2006), Pliocene changes in tropical east Pacific upper ocean stratification: Response to tropical gateways?, *Proc. Ocean Drill. Program: Sci. Results*, *202*, 1–51, doi:10.2973/odp.proc.sr.202.211.2006.

Steph, S., et al. (2010), Early Pliocene increase in thermohaline overturning: A precondition for the development of the modern equatorial Pacific cold tongue, *Paleoceanography*, *25*, PA2202, doi:10.1029/2008PA001645.

Toggweiler, J. R., K. Dixon, and W. S. Broecker (1991), The Peru upwelling and the ventilation of the South Pacific Thermocline, *J. Geophys. Res.*, *96*(C11), 20,467–20,497, doi:10.1029/91JC02063.

Tsuchiya, M., R. Lukas, R. A. Fine, E. Firing, and E. Lindstrom (1989), Source waters of the Pacific Equatorial Undercurrent, *Prog. Oceanogr.*, *23*(2), 101–147, doi:10.1016/0079-6611(89)90012-8.

Turk, D., M. J. McPhaden, A. J. Busalacchi, and M. R. Lewis (2001), Remotely sensed biological production in the equatorial Pacific, *Science*, *293*(5529), 471–474, doi:10.1126/science.1056449.

Turner, S. K. (2014), Pliocene switch in orbital-scale carbon cycle/climate dynamics, *Paleoceanography*, *29*, 1256–1266, doi:10.1002/2014PA002651.

Tziperman, E., and B. Farrell (2009), Pliocene equatorial temperature: Lessons from atmospheric superrotation, *Paleoceanography*, *24*, PA1101, doi:10.1029/2008PA001652.

Van Andel, T. H. (1975), Mesozoic/Cenozoic calcite compensation depth and the global distribution of calcareous sediments, *Earth Planet. Sci. Lett.*, *26*(2), 187–194, doi:10.1016/0012-821X(75)90086-2.

Wara, M. W., A. C. Ravelo, and M. L. Delaney (2005), Permanent El Nino-like conditions during the Pliocene warm period, *Science*, *309*(5735), 758–761, doi:10.1126/science.1112596.

Winckler, G., R. F. Anderson, M. Stute, and P. Schlosser (2004), Does interplanetary dust control 100 kyr glacial cycles?, *Quat. Sci. Rev.*, *23*(18), 1873–1878, doi:10.1016/j.quascirev.2004.05.007.

Winckler, G., R. F. Anderson, M. Q. Fleisher, D. McGee, and N. Mahowald (2008), Covariant glacial-interglacial dust fluxes in the equatorial Pacific and Antarctica, *Science*, *320*(5872), 93–96, doi:10.1126/science.1150595.

Wolff, E. W., et al. (2006), Southern Ocean sea-ice extent, productivity and iron flux over the past eight glacial cycles, *Nature*, *440*(7083), 491–496, doi:10.1038/nature04614.

Zhang, Z. S., K. Nisancioglu, M. Bentsen, J. Tjiputra, I. Bethke, Q. Yan, B. Risebrobakken, C. Andersson, and E. Jansen (2012), Pre-industrial and mid-Pliocene simulations with NorESM-L, *Geosci. Model Dev.*, *5*(2), 523–533, doi:10.5194/gmd-5-523-2012.

Ziegler, C. L., R. W. Murray, T. Plank, and S. R. Hemming (2008), Sources of Fe to the equatorial Pacific Ocean from the Holocene to Miocene, *Earth Planet. Sci. Lett.*, *270*(3–4), 258–270, doi:10.1016/j.epsl.2008.03.044.